Piecewise-linear Restoring Force Surfaces for Semi-Nonparametric Identification of Nonlinear Systems

Matthew S. Allen[1], Hartono Sumali[2] & David S. Epp[2]

[1]University of Wisconsin-Madison
535 ERB, 1500 Engineering Drive, Madison, WI 53706
Corresponding author, email: msallen@engr.wisc.edu, Tel: (608) 890-1619 Fax: (608) 263-7451

[2]Sandia National Laboratories*
P.O. Box 5800, Albuquerque, New Mexico 87185
hsumali@sandia.gov, dsepp@sandia.gov

Abstract:

A method for identifying a piecewise-linear approximation to the nonlinear forces acting on a system is presented and demonstrated using response data from a micro cantilever beam. It is based on the Restoring Force Surface (RFS) method by Masri and Caughey, which is very attractive when initially testing a nonlinear system because it does not require the user to postulate a form for the nonlinearity a priori. The piecewise-linear fitting method presented here assures that a continuous piecewise-linear surface is identified, is effective even when the data does not cover the phase plane uniformly, and is more computationally efficient than classical polynomial based methods. A strategy for applying the method in polar form to sinusoidally excited response data is also presented. The method is demonstrated on simulated response data from a cantilever beam with a nonlinear electrostatic force, which highlights some of the differences between the local, piecewise linear model presented here and polynomial-based models. The proposed methods are then applied to identify the force-state relationship for a micro cantilever beam, whose response to single frequency excitation, measured with a Laser Doppler Vibrometer, contains a multitude of harmonics. The measurements suggest that an oscillatory nonlinear force acts on the cantilever when its tip velocity is near maximum during each cycle.

Key words: nonlinear system identification; restoring force surface; micro electro-mechanical system; MEMS; nonlinear vibration; harmonic distortion; force state mapping.

* Sandia is a multi-program laboratory operated by Sandia Corporation, a Lockheed Martin Company, for the United States Department of Energy's National Nuclear Security Administration under Contract DE-AC04-94AL85000.

1. Nomenclature

w_L = Relative tip deflection, [m]
y = Absolute tip displacement, [m]
e_b = Base displacement, [m]
y_0 = Initial gap between beam and base, [m]
ω = Frequency, [rad/s]
ω_n = Natural frequency, [rad/s]
ζ = Damping ratio, [unitless]
f_{tot} = Total restoring forces [N]
f_{nl} = Nonlinear part of restoring forces [N]
m = Effective Mass [kg]
c = Damping Constant [N-s/m]
k = Stiffness [N/m]
ψ_n = n^{th} basis function for piecewise-linear function [unitless]
q_n = Coefficient of nth basis function [N or m/s^2]
N = Number of basis functions in piecewise-linear approximation
N_f = Number of time instants at which the acceleration, velocity and displacement are measured

2. Introduction

Among the multitude of nonlinear system identification methods in the literature, the Restoring Force Surface (RFS) method by Masri and Caughey [1] is particularly attractive because it can be used to obtain a nonparametric description of the nonlinear forces acting on a system. This allows one to address one of the primary difficulties encountered in nonlinear system identification, finding an appropriate mathematical form for the nonlinear system. The nonparametric restoring force surface can be examined to determine what mathematical form is appropriate, often yielding insight into the physics of the nonlinearity. One can then parameterize the RFS in order to condense the measured data and so the response of the system to other kinds of inputs can be predicted. This parameterization is typically done using a polynomial model for the nonlinear function, yet polynomial models can be numerically ill conditioned when their order is high, so it can be difficult to estimate their parameters. Orthogonal polynomial formulations are available that minimize numerical ill-conditioning at the expense of increased complexity in their implementation. Even if these difficulties can be addressed, the coefficients of the polynomials remain difficult to interpret physically, especially when their order is high.

This work describes a method for finding a piece-wise linear approximation to a set of restoring force surface data. This method uses finite-element-type shape functions to assure that the restoring force surface representation is continuous, and the shape functions are chosen so that all except for one are zero

at each node, so their coefficients are easily interpreted. Furthermore, the method is very computationally efficient, so this method may be useful for condensing a set of measured data even if the model form is known a priori; one could use this method to condense the measured data initially and to gain insight into the system's response, and then subsequently fit a model of the desired form.

Another issue encountered when applying the restoring force surface method is that it can be difficult to design an excitation signal that ensures that the response covers the phase plane entirely and uniformly. Sinusoidal excitation signals will almost certainly not result in uniform coverage of the phase plane, yet they are attractive for a number of other reasons. This work addresses the issue by implementing the piecewise-linear restoring force method in polar form; the restoring force is parameterized as a piecewise-linear function along its orbit in the phase plane.

Duym, Schoukens and Guillaume [2] previously presented a method that is similar to this work, in which they identified a local approximation to a restoring force surface over cells in a rectangular grid. In their work, each cell was defined by a small range of displacement and velocity. They presented a zero-order method that estimates the mean value of the restoring force over the cell and a first-order method that estimates the mean value and slope in two directions over the cell. Each unit cell was uncoupled from all others, so its mean restoring force (and slopes for the first order method) could be estimated independently using only the data that pertained to that unit cell. Presumably, this approach was adopted to maximize the computational efficiency of the algorithm, appropriate for the computing resources of the day. Unfortunately, their approach can result in a discontinuous surface, which is undesirable since the restoring force surfaces of interest in most problems are continuous. In their work it appears that they plotted their zero order surfaces as smooth surfaces by simply interpolating between the mean values estimated for each cell, yet this representation of the data is misleading since a stepwise surface with constant restoring force in each cell is what was actually computed. The error associated with using Duym, Schoukens and Guillaume's stepwise surface can be reduced by shrinking the size of the unit cells, yet in practice this inevitably results in some unit cells containing very little data or no data at all, which in turn can lead to an artificially rough estimate of the restoring force surface. Such an approach is sometimes adopted in the literature when displaying restoring force data [3]. The true-piecewise linear restoring force method presented here allows one to use a coarser grid, so it offers significant advantages when the measured data

is not uniformly distributed in the phase plane, and the surface identified is continuous, as one would expect for most real systems.

The proposed methods will be demonstrated on response data from a micro-cantilever beam manufactured using the Sandia Ultra-planar Multi-level MEMS Technology (SUMMiT^{TM}) manufacturing process. The responses of many of these micro-cantilever beams, measured with a Laser Doppler Vibrometer (LDV), have been found to exhibit significant nonlinearity, even when the tip displacement is less than 0.5% of the beam length and less than 50% of the beam height. The nonlinear forces acting on the beams appear to be quite complicated, as will be demonstrated later, and neither the mathematical form nor the cause of the nonlinearity is known, so the piecewise-linear method is attractive. This work is part of an effort to understand and model the nonlinearity in these MEMS systems. Worden and Tomlinson [4] and Kerschen *et al.* [5] successfully identified a model for a nonlinear, macro-scale cantilever beam using the restoring force surface method. The authors are not aware of a prior work in which the RFS method has been applied to a MEMS system using Laser Doppler Vibrometry.

A number of tests have been performed as part of this effort. The tip velocity of the beams was measured in near vacuum (~10 mTorr pressure) using a Laser Doppler Vibrometer (LDV) while the base of the beams was excited with a piezoelectric actuator. A second LDV was used to record the base velocity simultaneously. The bandwidth of the base excitation was limited to frequencies around the first resonance so the system would behave as a single degree of freedom. The restoring force surface method was then applied with the aide of the piecewise linear surface fitting approach. This was valuable in the present study because the cause of this nonlinearity is not known and tests with sinusoidal excitation show that the nonlinear dependence is complex, so traditional methods that rely on capturing nonlinearity with a low order polynomial series would be inefficient and possibly suffer from numerical ill-conditioning.

The following section provides a brief derivation of the restoring force surface method and presents the proposed piecewise-linear surface fitting method. Section 4 discusses the cantilever beam system of interest. Simulation results for a simplified model of the beam are presented in Section 4.1 in order to demonstrate the piecewise linear method. The actual experimental setup, test procedure and results are described in Section 4.2. Section 5 presents some conclusions.

3. Restoring Force Surface Method

The restoring force surface (RFS) method is simply an expression of Newton's second law for a single-degree of freedom, lumped mass system; the net force applied to a point mass is equal to its mass times its acceleration. For example, consider a single degree of freedom system with mass m, damping c, and stiffness k, that is acted on by nonlinear forces $f_{nl}(x,v)$ that are a single-valued function of the displacement x and velocity v given in the following equation of motion

$$m\dot{v} + cv + kx + f_{nl}\left(x, v\right) = f_{app} \tag{1}$$

where f_{app} is the external force applied to the system. All of the displacement and velocity dependent forces, or the restoring forces are collected as follows

$$m\dot{v} = -f_{rest}\left(x, v\right) + f_{app} \tag{2}$$

where the restoring forces are $f_{rest}(x,v) = cv+kx+f_{nl}(x,v)$. If the applied force and the acceleration are measured and the mass is known then the restoring forces can be found from Equation (2) as follows

$$f_{rest}\left(x, v\right) = -m\dot{v} + f_{app}\,. \tag{3}$$

The functional relationship between the force and displacement and velocity can be easily evaluated if the velocity and displacement can also be measured or estimated. These are both typically estimated from the measured acceleration [6].

One important consideration here is how the mass is estimated. A number of researchers have discussed methods for identifying the system mass [2, 7], so this will not be treated here. This is not an issue in the application of interest in this work, where base excitation is used, because base excitation results in the mass simply scaling the resulting forces. It will be taken to be unity since our objective is to obtain the functional form of the nonlinear forces; finding the precise magnitude of the forces is a secondary consideration. The term "restoring force" will be used to denote the unscaled acceleration since this is equal to the restoring forces after scaling by the constant unknown mass.

One drawback to the RFS method is that it is limited to single-degree of freedom or lumped parameter multi-degree of freedom systems [7]. In the application presented in this work, a single mode dominates the response so the RFS method is applicable. Kerschen et al. [6] recently presented an excellent summary of these and many other nonlinear system identification algorithms. The restoring force surface method is discussed in more detail in [1, 2, 6-8] and their references.

3.1. True Piecewise-Linear Restoring Force Surface

A true piecewise linear restoring force surface is found by parameterizing the surface using a set of local basis functions and then solving for the coefficient of each basis function, analogous to what is done in the now ubiquitous Finite Element Method. Consider a two dimensional restoring force surface $f(x,v)$ parameterized by basis functions $\psi_n(x,v)$ with coefficients q_n as follows.

$$f(x,v) = \sum_{n=1}^{N} q_n \psi_n(x,v) \tag{4}$$

A multitude of choices exist for the basis functions $\psi_n(x,v)$. Polynomial functions are commonly used. However, they can lead to numerical ill conditioning and can be sensitive to noise. This work concentrates on local basis functions since their coefficients q_n can be determined in a computationally efficient manner and because they do not require that one know the form of the nonlinear restoring force surface a priori.

For simplicity, the problem of identifying a one dimensional restoring force $f(x)$ will first be addressed. One first defines a set of nodes $(x_c)_n$ over the range of the function that one wishes to approximate. The spacing between each node and the next node need not be constant, yet it should be small enough to capture the variation in the function. Let Δx_n^- and Δx_n^+ denote the spacing between node n and the previous and next nodes respectively. Each node is then assigned the following shape function.

$$\psi_n(x) = \begin{cases} \left(x - \left(x_c\right)_n\right) / \Delta x^-_n & \left(x_c\right)_n - \Delta x^-_n < x < \left(x_c\right)_n \\ 1 - \left(x - \left(x_c\right)_n\right) / \Delta x^+_n & \left(x_c\right)_n < x < \left(x_c\right)_n + \Delta x^+_n \end{cases} \tag{5}.$$

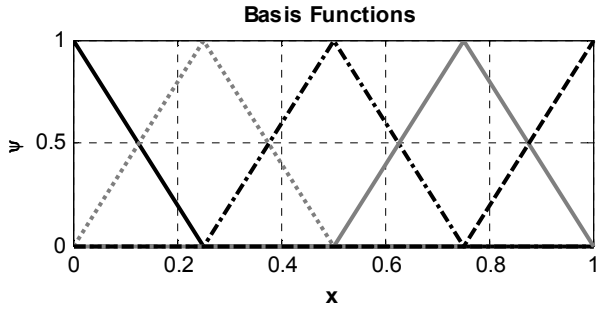

Figure 1: Sample basis functions for piecewise linear restoring force method for x ∈ (0,1).

A set of five sample basis functions are illustrated in Figure 1. Each basis function is simply a triangle function that starts at zero at the previous node, rises linearly to one at its node, and then falls off linearly between its node and the next. The basis functions pertaining to the extremes of the restoring force surface have similar form but are defined over a range Δx_n, using only one of the two definitions in

Equation (5) so that the restoring force is allowed to end with a non-zero value at the extremes of the measurement range. This eliminates any end effects that might contaminate the estimate of the value of the force at the end node points.

Because non-uniform grid points can be used, one can focus the mesh at points where the restoring force is discontinuous or rapidly changing with x. In the experimental application presented in this work, a uniform grid was defined spanning the range of the experimental measurements. Some of the nodes for the grid ended up belonging to basis functions that were defined over a range of x and y that contained little or no data. These points were discarded and the values of Δx_n for neighboring nodes updated, preserving a piecewise linear function on a non-uniform grid.

The coefficients of the basis functions are computed by setting up the following over-determined linear system using each measured force value $f(x_j,y_j)$.

$$f\left(x_i\right)=\begin{bmatrix}\psi_1\left(x_i\right) & \psi_2\left(x_i\right) & \cdots & \psi_N\left(x_i\right)\end{bmatrix}\begin{bmatrix}q_1\\ \vdots\\ q_N\end{bmatrix} \tag{6}$$

This equation can be written for each data point $f(x_i)$ for i=1...N_f, resulting in an over determined linear system of equations that is solved in a least squares sense. Each basis functions is defined over a local cell in the phase plane, so the matrix formed by stacking rows of Equation (6) will be sparse. Note that the cells for adjacent basis functions overlap, so the cells are not completely uncoupled as in [2] This sparsity can be exploited to create a computationally efficient algorithm by forming the normal equations associated with the least squares problem as follows.

$$\begin{aligned}\left(A^T B\right)_m &= \sum_{i=1}^{N_f} f\left(x_i\right)\psi_m\left(x_i\right)\\ \left(A^T A\right)_{m,n} &= \sum_{i=1}^{N_f}\psi_m\left(x_i\right)\psi_n\left(x_i\right)\end{aligned} \tag{7}$$

where m and m,n denote the m^{th} element and the m,n^{th} element of the vector A^TB and matrix A^TA respectively. These sums can be evaluated efficiently by noting that the products will be zero if the point x_i to which the force $f(x_i)$ pertains is not within the cell affected by the basis function $\psi_m(x_j)$ in the first equation and similarly for the pair of basis functions in the second equation. Furthermore, one need only

compute the sum for the data points for which one (or both) of the basis functions is nonzero. The coefficients of the basis functions are then found using the standard formula for the least squares solution.

$$q = \left(A^T A\right)^{-1} A^T B \tag{8}$$

The matrix $(A^T A)$ will be invertible if the basis functions are linearly independent and the data sufficient to adequately describe each basis function. The authors implemented the algorithm by discarding any nodes that were associated with less than one percent of the average number of data points associated with each node.

The method is easily extended to two dimensions by defining a similar set of basis functions in two dimensions

$$\psi_{m,n}(x,v) = \psi^{(x)}{}_m(x)\psi^{(v)}{}_n(v)$$

$$\psi^{(x)}{}_m(x) = \begin{cases} \left(x - \left(x_c\right)_m\right) / \Delta x^-{}_m & \left(x_c\right)_m - \Delta x^-{}_m < x < \left(x_c\right)_m \\ 1 - \left(x - \left(x_c\right)_m\right) / \Delta x^+{}_m & \left(x_c\right)_m < x < \left(x_c\right)_m + \Delta x^+{}_m \end{cases} \tag{9},$$

where the v-direction basis function $\psi^{(v)}{}_n(v)$ is obtained by replacing x with v in the previous equation. The basis functions are once again unity at a single node point $((x_c)_n, (v_c)_n)$ on a grid. In this case the total number of basis functions in Equation (9) will be the product of the number of basis functions in x and v.

In the work presented in Section 4.2, a micro-cantilever beam was excited with base excitation. The measured data were the base velocity and tip velocity. The base velocity was sinusoidal with varying amplitude. In each period in the steady state, the tip velocity was nearly sinusoidal. As a result, the phase plane was populated with data points only in a region close to an orbit. Therefore, a two-dimensional RFS on a rectangular grid was not optimal because many of the grid points ended up being in regions of the phase space that were devoid of data. In the following a *one dimensional* piecewise linear approximation is found for: 1) the restoring force, 2) the tip displacement and 3) the tip velocity, all as a function of the phase angle of the base velocity. This information was then used to construct the two-dimensional RFS in polar form.

4. Application

Figure 2 shows a schematic of the system under study consisting of a cantilever beam attached to a moving base. The beam is excited around its first resonance, so assuming that modal coupling is negligible

(as will be illustrated subsequently), it can be approximated as a single oscillator subject to base excitation. The oscillator is assumed to be connected to its base by a nonlinear element resulting in the following differential equation

$$m\ddot{y} + c\dot{y} + ky + f_{nl}\left(\dot{w}_L, w_L\right) = c\dot{e}_b + ke_b \tag{10}$$

or

$$m\ddot{y} = -f_{rest}\left(\dot{w}_L, w_L\right), \tag{11}$$

Where y is the absolute displacement of the tip of the beam, c and k are respectively the damping and stiffness between the beam tip and the moving base and f_{nl} represents the nonlinear restoring forces that are assumed to depend only on the displacement of the beam tip relative to the substrate w_L and its derivative

$$w_L = y - e_b \tag{12}.$$

The effective mass of the single degree of freedom representation for the cantilever is m.

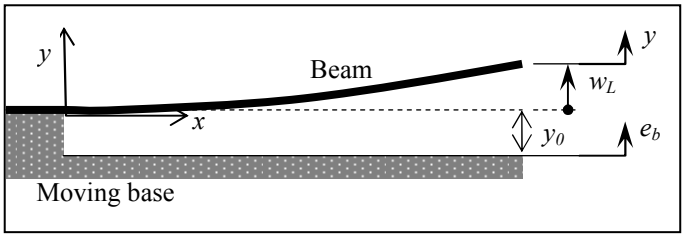

Figure 2: Schematic of the system under study.

An array of micro cantilever beams was created using Sandia National Laboratories' SUMMiT^{TM} process on a silicon wafer. This work is concerned with a beam that had nominal length of 200 μm, width of b_{beam} = 10 μm and height of 2.5 μm. It was fixed to the substrate at one end and free at the other. The beam was constructed by depositing two poly-silicon layers of thicknesses 1.5 μm and 1.0 μm over a 2 μm layer of sacrificial oxide and then removing the oxide. Figure 3 shows an optical microscope image of an array of beams, including the beam for which results are presented in Section 4.2. Additional poly-silicon layers were placed over the root of the array of beams, as seen in Figure 3. A 0.3 μm layer of poly-silicon was deposited under the root of the beams to allow for electrostatic actuation, causing a 0.3 μm step in the profile of the beam since the layers are conformal, as can bee seen in Figure 3.

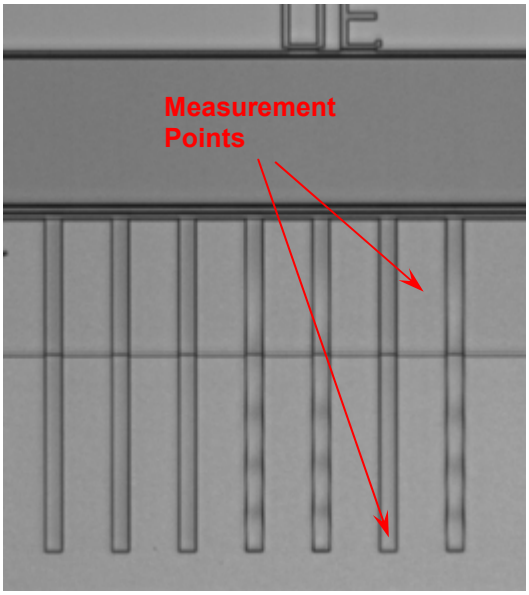

Figure 3: Optical microscope image of micro-cantilever beams.

4.1. Analytical Model

A simple model of the cantilever of interest was created and its response simulated to demonstrate the performance of the piecewise-linear restoring force surface algorithm. The beam was modeled as an ideal Euler-Bernoulli cantilever beam with nominal dimensions and Young's modulus E = 170 GPa and density ρ = 2330 kg/m^3. A single-term Ritz model for the beam was constructed using the method in Ginsberg [9]. Base excitation of the beam was of interest, so Ginsberg's method for accounting for time varying boundary conditions was applied to the displacement boundary condition at the clamped end of the cantilever. A nonlinear electrostatic attractive force between the beam and substrate was also simulated, by applying the following distributed load *f(x)* to the beam that depends nonlinearly on the deflection of the beam from its undeflected position *w(x)*.

$$f(x) = \frac{-0.5\varepsilon_0 b_{beam} V^2}{\left(y_0 - w(x)\right)^2} \tag{13}$$

where ε_0 = permittivity of free space = 8.85*10^{-12} [C^2/(Nm^2)], V = voltage [Volts], y_0 [m] is the distance between the beam and the base when the beam is undeflected and b_{beam} [m] was defined previously. Values of V = 7 Volts and y_0 = 1.5 μm were used in the following simulation and the damping constant of the Ritz model was set to give a linear damping ratio of 0.1%.

The response of the cantilever to sinusoidal base excitation at 73 kHz with 50 nm amplitude was simulated using an adaptive Runge-Kutta algorithm. The simulated restoring was found from the simulated beam tip displacement and acceleration and is shown in Figure 4. The restoring forces of this simulated system depend only very weakly on velocity due to the lightness of the damping that was used, so their dependence on tip velocity has been ignored.

Both 2nd and 3rd order polynomial models were fit to the simulated data as a function of tip displacement, as well as a piecewise linear model. The displacement was first scaled to the interval $-1 \leq w_L \leq 1$ prior to fitting the polynomial models in order to minimize numerical ill-conditioning. The nodes of the piecewise linear model were unevenly distributed to concentrate them at large negative displacements, where the restoring force is most nonlinear. The polynomial models disagree with the data in the region where the nonlinearity is largest, although the disagreement is less for the 3rd order polynomial than for the 2nd order one. The piecewise-linear model follows the data precisely, even in the region where the nonlinearity is largest, due to the fineness of the mesh employed in the nonlinear region.

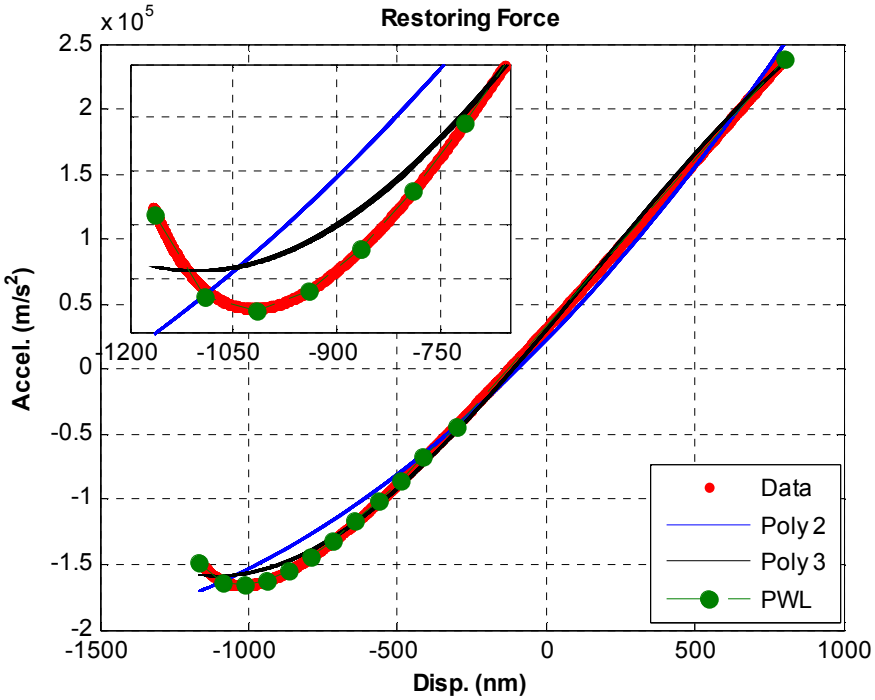

Figure 4: Simulated restoring force for cantilever beam with electrostatic attractive force: (red circles) simulated data, (blue line) 2nd order polynomial fit to simulated data, (black line) 3rd order polynomial fit to data, (green line) piecewise-linear fit to data, (green circles) nodes of the PWL model.

4.1.1. Discussion

This example illustrates some of the differences between the piecewise-linear restoring force surface and the traditional polynomial based RFS. The polynomial model in this example converges to the measured restoring force as its order is increased. Each polynomial term depends on the entire measured data set, so convergence is global and so one may observe regions of the phase space where the convergence is not adequate if the polynomial order is not high enough.

In contrast, the piecewise-linear model is a local model; the value of the piecewise-linear approximation at each node depends only on the data immediately before and after each node. Hence, each node tends to give a good approximation of the average value of the measured restoring force in its vicinity. As with the finite-element method, one can refine the mesh used in the piecewise-linear approximation non-uniformly to better describe local features of a nonlinear force-displacement relationship without encountering numerical ill conditioning.

This simple example has not illustrated the effect of measurement errors on these two methods, yet they can have a considerable effect in practice. For example, signal processing can introduce outliers, or the measurement system may distort data near the extremes of the phase plane. One consequence of the fact that the polynomial basis functions are global is that errors in the measured data that affect only a small portion of the phase plane can cause global changes in the polynomial model, perhaps even rendering it useless. This problem is exacerbated when numerical ill-conditioning is encountered, since it tends to increase the sensitivity of the polynomial model to small changes in the measurements. On the other hand, a localized error in the measurements affects only the corresponding local portion of the model when the piecewise-linear algorithm is used.

4.2. Experimental Test Procedure

This section describes the results of tests on the silicon micro-cantilever beams that were described previously. As mentioned previously, electrostatic actuation pads were manufactured under each beam. However, the beams were found to respond in a highly nonlinear manner even when no voltage difference was applied between the actuation pads and the beams. For this reason, electrostatic actuation was not used in this study in order to focus on the nonlinearity of the beams alone. This section presents the results of

testing the single beam indicated in Figure 3 using base excitation in the absence of an applied electrostatic voltage.

The beams were fastened to a piezoelectric actuator, which was itself fastened to a steel block that served as a seismic mass. The assembly was then placed in a vacuum chamber and the air in the chamber was evacuated resulting in a test pressure of about 10 mTorr. Laser measurements were obtained by imaging through a quartz window.

The base of the cantilever was driven by applying an 82 kHz sinusoidal voltage to the piezoelectric actuator with amplitudes ranging from 0-20 Volts, corresponding to near-resonant excitation. 524288 samples of the beam tip and substrate time responses were recorded, at 5.12 MHz. The laser hardware includes a low-pass anti-aliasing filter with a cutoff frequency of 1.5 MHz.

The base velocity and the velocity of the tip of the beam were both measured using a Polytec Laser Doppler Vibrometer (LDV) focused through a Mitutoyo optical microscope with a 10X objective lens. The velocities were integrated and differentiated using variations on the technique described by Smallwood [10]. The restoring force, found using Equation (11) as the derivative of the measured tip velocity, will be evaluated as a function of the relative tip displacement w_L and its derivative $\dot{w}_L$. The relative displacement and relative displacement velocity, w_L and $\dot{w}_L$, were found by taking the difference between the integrated and measured tip and base velocities. All of the signals were high-pass filtered with an 8th order Butterworth filter with a cutoff frequency of 40 kHz to eliminate the spurious drift caused by the laser.

4.2.1. Experimental Results

The autospectra of the tip velocities of this beam for various excitation amplitudes are displayed in Figures 5 and 6. All of the autospectra are dominated by an 82 kHz sinusoid, and all show multiple harmonics, some of whose magnitudes are only 15-20 dB below the fundamental. (The autospectrum is squared quantity so a harmonic that is 20dB below the fundamental would have a velocity amplitude that is 10% that of the fundamental 82 kHz sinusoid.) Markers are shown for each curve indicating the peak nearest to a multiple of the 82 kHz drive frequency. The base autospectra are not shown, yet in each case they were a pure 82 kHz sinusoid with 40 dB or so lower amplitude than the tip. No harmonics were

visible in the base autospectra above their noise floor, which was at about the same level as the tip autospectra's noise floor.

Figure 5 shows that the bandwidth of the harmonics increases with increasing excitation amplitude, continuing out beyond the 1.5 MHz cutoff frequency of the laser decoder for higher excitation amplitudes. Other peaks are also evident at frequencies that are not integer multiples of the excitation frequency. For example, there are peaks at 520 kHz and 1450 kHz. If the beam were an ideal Euler-Bernoulli cantilever with nominal cross sectional properties one would expect the first three modal frequencies to be 81.1, 508 and 1423 kHz [9]. The peaks at 520 and 1450 kHz are 30-40 dB or more below the response at the excitation frequency and about 20 dB below the harmonics at most amplitudes, so their effect on the response is expected to be small relative to the nonlinear response. The 130 nm and 270 nm tip amplitude cases are the exception having responses at 520 and 1450 kHz that are only 10-15 dB below the dominant harmonics. It was also noted that the restoring force surface data at 130 and 270 nm tip amplitudes had the largest variability with respect to the base phase.

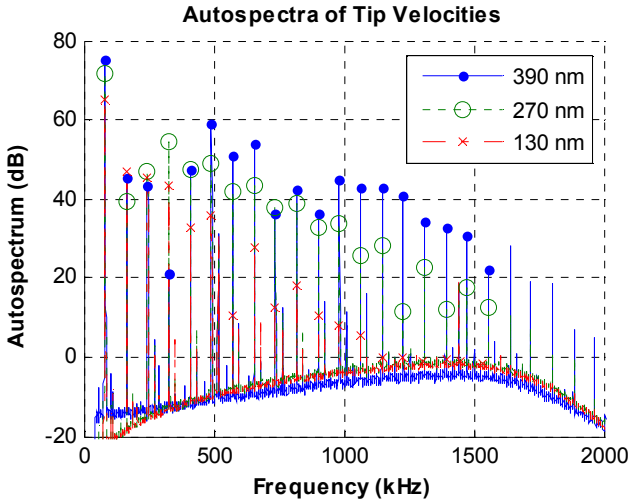

Figure 5: Autospectra of tip velocities for 130, 270 and 390 nm tip amplitudes. (0dB = 0.034 mm/s)

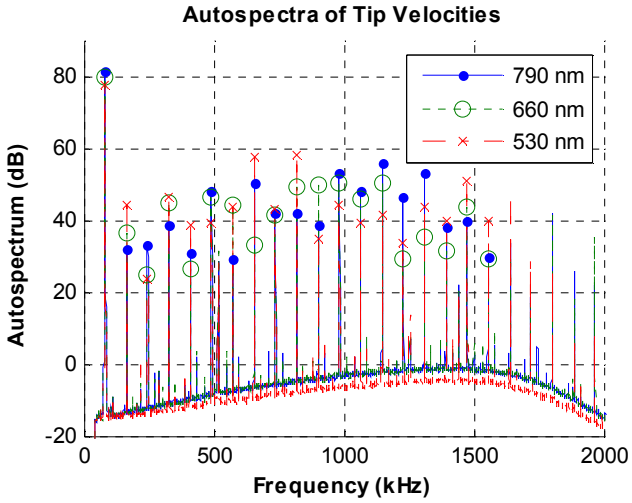

Figure 6: Autospectra of tip velocities for 530, 660 and 790 nm tip amplitudes. (0dB = 0.034 mm/s)

The restoring force surface values for 2500 samples of each response are displayed in Figure 7, with the value of the restoring force indicated by the color of the circles. Note that the restoring force, found using Equation (11), can be evaluated at any pair of values $\left(w_L, \dot{w}_L\right)$ where the response has been measured. One should note that the beam is very lightly damped, and near resonant excitation results in the tip motion being about 100 times larger than the base motion, so the base motion has a miniscule contribution to the restoring force in Equation (11). (The actual Q of the beam, found in other tests using broadband excitation, is about 5000, corresponding to a damping ratio of ~0.01%.) Figure 7 shows the restoring force only at the points in the $\left(w_L, \dot{w}_L\right)$ plane through which the response passes during the first 2500 samples for various excitation amplitudes. Different rings correspond to the following piezo excitation amplitudes 3.3V, 6.6V, 10V, 13.3V, 16.6V and 20V. These resulted in approximately 130, 270, 390, 530, 660, and 790 nanometers peak tip displacements. Multiple data sets are shown for most of the amplitudes, illustrating the level of repeatability observed in the measurements. The measurements at amplitudes below 600nm are all highly repeatable, whereas the different trials for peak amplitudes above 600nm show significant variation. The orbits traced in the phase plane at each amplitude also differ from the pure elliptical motion expected for a linear time invariant system. This deviation takes the form of ripples in the rings at the points where the magnitude of the velocity is largest, although the velocity at which the rippling begins changes with differing excitation amplitude.

The colored circles indicate a clear linear trend in the restoring force surface for increasing displacement (w_L), suggestive of an underlying linear stiffness. At moderately high amplitudes the restoring force changes sign a number of times as the cantilever tip executes one vibration cycle. The ripples in the restoring force appear to occur only when the tip velocity is relatively high. The restoring force at the two highest amplitudes is clearly multi-valued, while at other amplitudes the measurements are highly consistent. A multi-valued RFS suggests that the force is altered by effects other than the tip displacement and velocity. We wish to investigate this in more detail by characterizing the RFS at lower amplitudes and then comparing it to that obtained when other types of excitations are used. Without some kind of parameterization, the data in Figure 7 could not be used to reconstruct the response of the cantilever to other inputs. This restoring force surface is not amenable to any simple representation, so the piecewise linear method presented previously is attractive.

It is important to note the dependence of the restoring force on both displacement and velocity in Figure 7. The response at each amplitude traces a distorted ring in the phase plane, and the rings are such that the large amplitude response cannot be predicted simply by stretching the ring obtained at low amplitude or vice-versa. Hence, it will be necessary to first parameterize the restoring force as a function of displacement and velocity for each tip amplitude independently. The responses at different amplitudes can then be stitched together to find a general model for the nonlinearity.

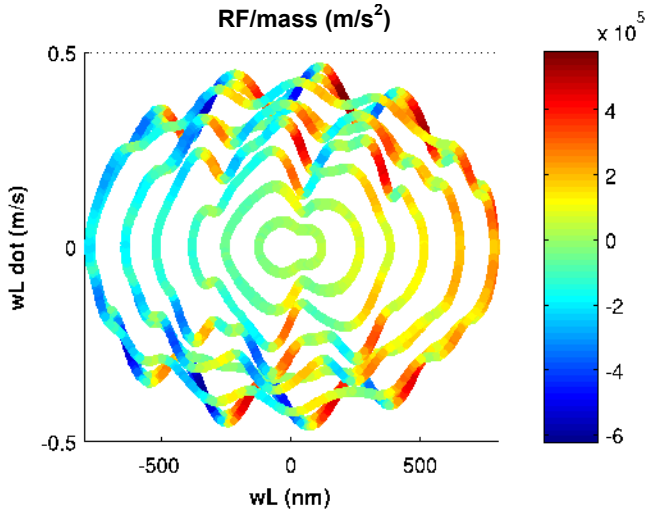

Figure 7: Scatter-plot of restoring force surface

One can capitalize on the periodic nature of the data to simplify the system identification procedure. First recognize that the data is periodic with period of $1/f_d$ seconds, where f_d is the drive

frequency, so the phase variable θ can be constructed from the drive frequency, time (t) and phase delay (ϕ_{delay}) as

$$\theta = 2\pi f_d t - \phi_{delay} \tag{14}.$$

The phase delay is found such that the base velocity is a pure sinusoid. The phase angle can then be wrapped to the interval [0,2π) by subtracting off integer multiples of 2π. The restoring force, tip displacement (w_L) and tip displacement velocity ($\dot{w}_L$) can each then be found as a function of the phase angle θ.

Figures 8 and 9 show the measured restoring force and piecewise linear fits for 130 and 530 nm tip amplitudes respectively. The top subplot shows the measured restoring force versus phase angle for two different data sets (blue and green points) and the piecewise linear fit to the combined set of data (red line). The two independent data sets are highly consistent at both amplitudes, and the piecewise linear approximation fits them well. The data at 130 nm amplitude shows considerably more scatter, yet the piecewise linear fit follows the mean trend of the data well. These data sets are representative of the best and worse agreement found below 530 nm tip amplitude.

The bottom two subplots in Figures 8 and 9 show the piecewise linear fits for the relative tip displacement (nm) and relative tip velocity (mm/s). The data from which these fits were derived is not shown, yet it was noted that there was considerably less scatter in the displacement and velocity data than there was in the restoring force data shown in Figures 8 and 9, so the fit to the velocity was almost indistinguishable from the average of the measured relative velocity. Hence, the velocity traces in Figures 8 and 9 essentially show the average measured response over one cycle and illustrate the degree of harmonic distortion in the measured velocity-time traces, which is quite severe at high amplitudes. Finally, it is apparent that the 130 nm amplitude RFS is not simply a subset of the 530 nm RFS, as one would expect if the nonlinearity were primarily a function of displacement; both displacement and velocity contribute to the observed nonlinearity.

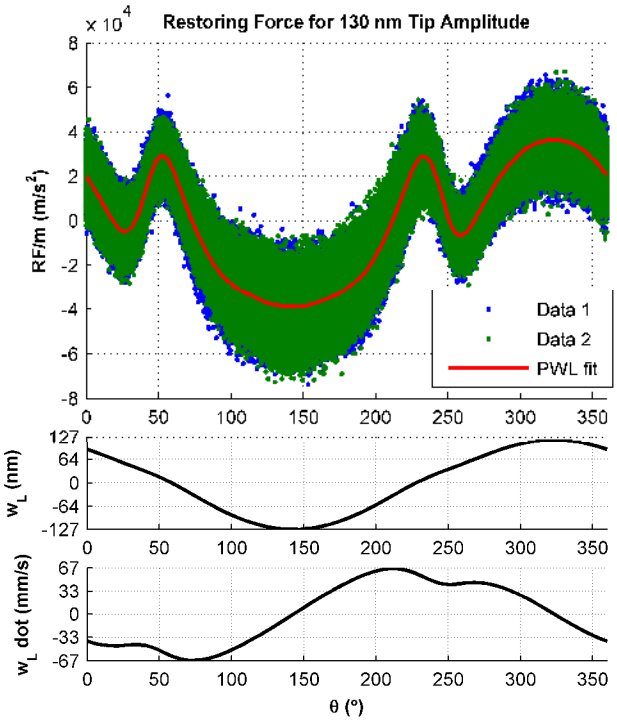

Figure 8: Restoring force data versus phase angle for two data sets and piecewise linear fit at 130nm tip amplitude.

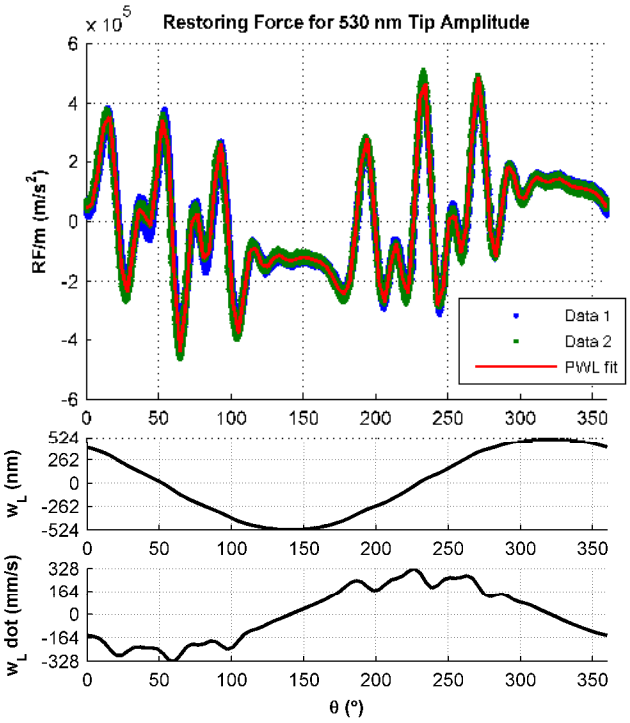

Figure 9: Restoring force data versus phase angle for two data sets and piecewise linear fit at 590nm tip amplitude.

The piecewise linear fits were then used to construct the restoring force surface for a range of amplitudes by linearly interpolating between amplitudes at the same phase angle. Figure 10 shows the result for low excitation amplitudes (i.e. using only the piecewise linear fits for 130, 270 and 390 nm tip amplitude.) The surface is highly irregular, especially at high tip velocities where the restoring force oscillates within each cycle.

At low velocities the force appears to be somewhat linear, so this data could be consistent with a nearly linear static force-displacement curve. This is examined in more detail in Figure 11, where the data from Figure 10 with tip displacement velocity ($\dot{w}_L$) near zero is plotted versus w_L. This is essentially a zero velocity slice of the surface. Different markers are used for each tip amplitude so they can be distinguished. The data agree very well with the linear stiffness line (red dash-dot) that one would predict for an Euler-Bernoulli cantilever beam with nominal stiffness, density and dimensions (first resonant frequency of 81.1 kHz).

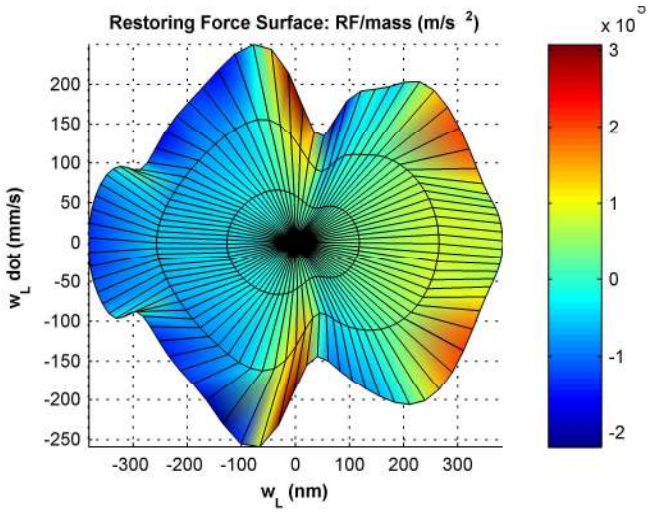

Figure 10: Restoring force surface versus tip displacement and velocity at low excitation amplitudes.

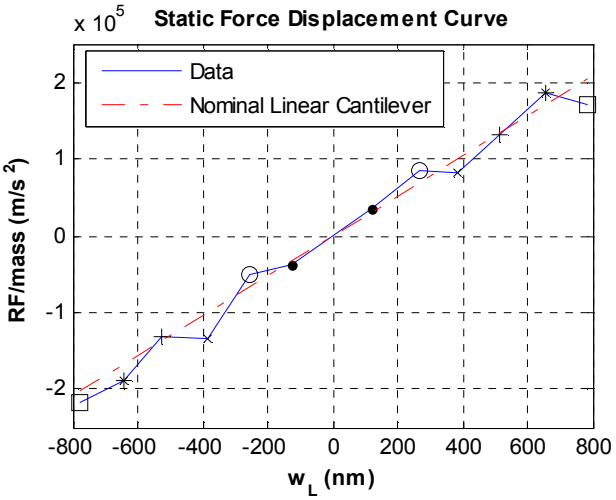

Figure 11: Static force-displacement curve for micro-cantilever beam, derived from restoring force surface data in Figure 10. The markers indicate the amplitude of excitation from which each pair of data points was derived.

4.2.2. Discussion

One convenient feature of sinusoidal excitation is that it allows one to easily detect nonlinearity; responses at frequencies other than the driving frequency indicate nonlinearity. The autospectra in Figures 5 and 6 show that the system response is clearly nonlinear, and suggest that the nonlinearity is responsible for as much as 10% of the velocity response at some frequencies. It is important to verify that the laser Doppler vibrometer measurement system is behaving linearly before attributing this nonlinearity to the micro-cantilever beams, otherwise one might be measuring the nonlinearity of the combined LDV-cantilever beam system. (If the LDV were in fact nonlinear, such a measurement might be useful for understanding why, yet it was not the purpose of this study.) In order to assure that the measurements are correct, the tests were replicated with other laser decoder range settings and identical results were found. Also, it was verified that the measured velocities were no higher than 500 mm/s while Polytec's specifications state that the instrument nonlinearity should not exceed 1% for velocities up to 1500 mm/s for the range settings that were used. These observations suggest that the measured responses are not an artifact of the laser measurement system. Also, the response deviates from a pure sinusoid most strongly when the velocity is highest, as illustrated in Figure 7; if there were difficulty with the laser measurement system, one would expect it to occur at low velocities rather than at high velocities as observed. These observations suggest that the beams may in fact be behaving nonlinearly, even though their tip deflections are less than their thickness.

Figure 9 shows that the magnitude of the nonlinear forces acting on the cantilever are much larger than those of the linear forces at some points in the cycle. The restoring forces presented in Figures 7 and 10 are not amenable to any simple force versus displacement model. Indeed, the autospectrum in Figure 5 shows more than 19 harmonics, so one might need as many as 19 terms to describe the restoring force using a polynomial series. In fact, the authors initially attempted using a low order polynomial series both with the RFS method and with the Reverse Path [11] method and were not able to find a model that fit the data even reasonably well. Higher order polynomial models were impractical due to the computational burden they required and numerical ill conditioning. On the other hand, it was a relatively simple matter to fit a piecewise-linear restoring force surface to the data, and this was done very comfortably on a standard desktop computer. Furthermore, the piecewise-linear restoring force surface always tracked the mean value of the measurements whereas the polynomial models investigated by the authors always deviated from the data wildly at some points in the phase plane. The piecewise-linear restoring force surface algorithm gives a compact and accurate model for the nonlinear restoring forces that could be used to simulate the response of the system to other inputs or evaluated to determine the origin of the nonlinear forces.

When considering the cause of the nonlinearity, there are a few nuances in the data that one should note. First, the restoring force found at 130 nm tip amplitude, shown in Figure 8, shows considerable scatter. It was also noted that the peaks in the autospectra of the velocity in the vicinity of the 2^{nd} and 3^{rd} natural frequencies of the beam were considerable relative to the nonlinear harmonics at this amplitude (and would be even more so in the acceleration). The presence of the 2^{nd} and 3^{rd} modes in the response contaminates the restoring force, and one could have notch or low-pass filtered the data to eliminate the effects of these modes, as done in [4, 5]. However, since these modes' frequencies are not integer multiples of the first natural frequency or the excitation frequency, their contributions average to zero over a sufficient number of cycles of the input. These modes appear to have had a smaller net effect on the data at higher excitation amplitudes.

Another interesting observation is that the autospectra in Figure 5 show that the beam responds out beyond the 1.5 MHz bandwidth of the laser decoder. Harmonics beyond the 19^{th} may contain important information about the restoring force surface that was not captured. (In such a case one would expect the measurements to reflect a truncated Fourier series type representation for the restoring force surface; the

omitted terms may alter the representation of the restoring force surface over the whole range of displacement and velocity.) On the other hand, the harmonics in the autospectra for small tip displacement amplitudes (130, 270 and 390 nm) had decayed significantly at 1.5 MHz, suggesting that the restoring force should have been adequately captured at these amplitudes. For this reason, the restoring force surface was only displayed for these amplitudes in Figure 10.

It seems that one important clue to the cause of the nonlinearity in these measurements is its velocity dependence. Figure 11 suggests that the force-displacement relationship is linear at zero velocity. On the other hand, Figure 7 shows that for any given amplitude, the response appears to be somewhat linear until a certain tip speed is reached, after which the response becomes erratic until the speed again falls below that threshold. The oscillatory nature of the response is reminiscent of a stick-slip phenomenon, in which the unmeasured state could be the state of an internal Jenkins element [12]. Somewhat similar oscillatory forces are presented in Figure 10a of [3] for a macro-scale system with Coulomb friction, yet the oscillations observed there were not as severe nor quite as regular. Considering the layer-wise manufacturing process for these cantilevers, it is perhaps possible that the structure contains regions where the interlayer adhesion is weak or has failed that could act as sliding surfaces. For example, there might be regions near the root where some of the sacrificial oxide remains that the poly-silicon beam could slide against. Even so, some of the phenomena observed cannot be explained by a single degree of freedom model with Coulomb friction, nor are the authors aware of an alternative sliding friction model that could describe this type of response. For example, neither Segalman's Iwan element [12] nor the Bouc-Wen model [3, 13] are capable of describing this oscillatory behavior at high velocities for a single degree of freedom system.

This paper presents test data from only one beam. The authors have measured qualitatively similar responses from other beams of lengths ranging from 100 - 1500 microns, widths ranging from 10 to 30 microns and similar thicknesses (1.5-2.5 microns). Although the cause of the nonlinearity has not yet been determined, the piecewise-linear restoring force surface method has proven helpful in condensing the measured data and eliminating a number of theories regarding the cause of the nonlinearity. Efforts are underway to develop a mathematical model that recreates the observed behavior. The authors are also investigating the LDV to verify that the manufacturer's specifications regarding its linearity are correct.

5. Conclusions

A semi-nonparametric extension to the restoring force surface method was presented that creates a piecewise-linear approximation to the restoring forces acting on a dynamic system. The sparsity of the problem was exploited, resulting in a highly efficient algorithm for condensing a set of measured data into a continuous, piecewise-linear function. The function found tends to track the mean of the measured data very well. In contrast, the authors have found that this is not always the case when using other standard model forms, such as polynomials, for the nonlinearity. This piecewise-linear method is also able to deal with data that is not uniformly distributed in the phase plane much more effectively than the method of Duym, Schoukens and Guillaume [2]. A methodology was also presented that can be used to extract a polar representation when dealing with sinusoidally excited data. The piecewise-linear model found using the methods presented here is valuable in guiding initial efforts aimed at finding a suitable mathematical form for a system or for condensing a set of measured data so that a suitable mathematical model can more easily be found.

The proposed method was demonstrated on a simple analytical beam with a nonlinear electrostatic force and using experimental measurements from a micro-cantilever beam that exhibits a complicated, velocity-dependent nonlinearity. The experimental beam was tested in vacuum and was excited by applying sinusoidal excitation to its base of varying amplitude. The restoring force surface (RFS) method was used to characterize the nonlinearity because it allows for nonparametric analysis of nonlinear response data. The RFS method provided powerful insight into the dynamics of this system, and a piecewise-linear approximation to the nonlinear forces was found that could be used to simulate the response of the system to different excitations or initial conditions. Future work will investigate whether the same low amplitude restoring force surface is obtained when different types of excitations, such as swept sine excitation are used.

6. Acknowledgements

The authors would like to thank Jon Whittwer for helpful discussions regarding the SUMMiT^{TM} process. This work was performed at Sandia. Sandia is a multi-program laboratory operated by Sandia Corporation, a Lockheed Martin Company, for the United States Department of Energy's National Nuclear Security Administration under Contract DE-AC04-94AL85000.

7. References

1. Masri, S.F. and T.K. Caughey, *A Nonparametric Identification Technique for Nonlinear Dynamic Problems.* Journal of Applied Mechanics, 1979. **46**: p. 433-447.
2. Duym, S.W.R., J.F.M. Schoukens, and P.A.N. Guillaume, *A local restoring force surface method.* The International Journal of Analytical and Experimental Modal Analysis, 1996. **11**(3-4): p. 116-132.
3. Caffrey, J.P., et al., *A Re-Configurable Test Apparatus for Complex Nonlinear Dynamic Systems.* Nonlinear Dynamics, 2004. **36**(2): p. 181-201.
4. Worden, K. and G.R. Tomlinson. *Experimental study of a number of nonlinear SDOF systems using the restoring force surface method*. 1991. Florence, Italy: Publ by Union Coll, Schenectady, NY, USA.
5. Kerschen, G., J.-C. Golinval, and K. Worden, *Theoretical and Experimental Identification of a Non-Linear Beam.* Journal of Sound and Vibration, 2001. **244**(4): p. 597-613.
6. Kerschen, G., et al., *Past, present and future of nonlinear system identification in structural dynamics.* Mechanical Systems and Signal Processing, 2006. **20**: p. 505-592.
7. Worden, K., et al., *Experimental Identification of Multi Degree-of-freedom Nonlinear Systems using Restoring Force Methods.* The International Journal of Analytical and Experimental Modal Analysis, 1994. **9**(1): p. 35-55.
8. Adams, D.E. and R.J. Allemang. *Survey of Nonlinear Detection and Identification Techniques for Experimental Vibrations*. in *International Seminar on Modal Analysis (ISMA 23)*. 1998. Leuven, Belgium.
9. Ginsberg, J.H., *Mechanical and Structural Vibrations*. First ed. 2001, New York: John Wiley and Sons. 691.
10. Smallwood, D.O., *Integration of Equally Spaced Sampled Data Using a Generalized Whittaker's Reconstruction Formula.* IEEE Transactions on Acoustics, Speech and Signal Processing, 1980. **ASSP-28**(3): p. 341-343.
11. Bendat, J.S., *Nonlinear System Techniques and Applications*. 1998: John Wiley & Sons, inc. 474.
12. Segalman, D.J., *A Four-Parameter Iwan Model for Lap-Type Joints.* Journal of Applied Mechanics, 2005. **72**(5): p. 752-760.
13. Masri, S.F., et al., *Identification of the state equation in complex non-linear systems.* International Journal of Non-Linear Mechanics, 2004. **39**(7): p. 1111-1127.